Electromagnetic Interruption Shielding Characterization Of Plain Barium Ferrite

Preeti Gairola

S. P. Gairola

B. M. S. Bisht

Anu Pande

Uttaranchal University, Prem Nagar, Dehradun, India

S. K. Dhawan

National Physical Laboratory (CSIR), K, S. Krishnan Marg, New Delhi, India

Kuldeep Singh

Central Electrochemical Research Institute Karaikudi, Tamilnadu, India

L. P. Purohit

Department of Physics, Gurukula Kangri Vishwavidyalaya, Haridwar, India

Sudesh Sharma

University of Petroleum & Energy Studies, Bidholi, Dehradun, India

Abstract: Barium ferrite nanoparticles (50–70) nm has been synthesized by citrate precursor method. The structures, morphology, of samples were characterized by powder Scanning electron microscopy (SEM), Transmission electron microscopy (TEM) and X-ray diffraction (XRD). Magnetic properties of Barium ferrites have been investigated by vibrating sample magnetometer (VSM) at room temperature and other properties like complex permittivity, permeability, and microwave absorption were studied in the 8-12 GHz X-band frequency range by vector network analyzer (VNA).

Keywords: Citrate precursor; Barium ferrite; VNA; Electromagnetic Shielding;

I. INTRODUCTION

With the advancement in wireless communication and defense industries, radar absorbing materials are becoming more important [1, 2]. Therefore, the microwave-absorbing materials with strong absorption over a broad frequency range are required to solve the EMI problem. Microwave shielding has been applied to various systems such as mobile phones, computers, and stealth technology. If the characteristic impedance of free space is matched with the input characteristic impedance of an absorber then EM wave energy can be completely absorbed and dissipated into heat through magnetic and dielectric losses. Over the past decades, ferroelectric materials [3, 4], ferrite absorbers [5–7], composite materials [8, 9] and conductive polymers [10–12], have been researched. Ferrites have been used as absorbing materials in various forms, e.g. ceramic tiles, films, paints, sheet, and powders mixed with conducting materials or load in matrix composites [13]. are used as EMI shielding materials (Soft magnetic metals) are used traditionally, but they are restricted by the eddy current [14, 15]. The Hexagonal barium ferrite $BaFe_{12}O_{19}$ is well known hard magnetic materials due to its excellent resistance to oxidation, high natural resonance frequency and wide bandwidth [16, 17]. Barium ferrite possesses relatively high coercive force, magnetic anisotropy field and Curie temperature as well as its excellent chemical stability and corrosion resistivity [18-22].

II. EXPERIMENTAL

A. MATERIALS

Barium Nitrate $Ba(NO_3)_2$ and Ferric Nitrate $Fe(NO_3)_3$ were acquired from Loba, India. Citric acid and Ammonium

hydroxide solution obtained from Merck, India were used as accepted without further purification.

B. SYNTHESIS OF NANOFERRITE

For the synthesis of barium ferrite, citrate precursor method was used. Ba(NO3)2, Fe(NO3)3 and citric acid were taken as beginning materials. Required amounts of Ba(NO3)2 and Fe(NO3)3 were dissolved in minimum amount of deionized water. The molar ratio of Ba to Fe was kept 1:12. An aqueous solution of citric acid was mixed with Nitrate solution [mixture of Fe (NO3)3 and Ba(NO3)2]. The molar ratio of total moles of nitrate ions to citric acid was fixed at 1:1. Ammonia solution was gradually added to balance the pH at 9. Finally the mixed solution was allowed to vaporize by heating at 100 °C with constant agitation. As water vaporized, the solution became viscous and finally brown gel was formed. With continuous heating and increasing the temperature, the gel bubbled in combustion manner to form a brown colored porous powder. This powder was calcinated at 900 °C for 2h in air to get the barium ferrite phase.

The resultant powder of the combustion was milled by mechanical ball mill. The ball-to-powder weight (gm) ratio was 10:1. The mixing was operated using hardened steel balls with a diameter of 10mm. The milling speed was 400 rpm.

III. MEASUREMENTS

The particle size of barium ferrite have been analyzed using high-resolution transmission electron microscopy (HRTEM, model Technai G2 F30 Stwin, USA) operating at an accelerating voltage of 300 kv and having a point resolution of 0.2 nm and a lattice resolution of 0.14 nm. EG and $BaFe_{12}O_{19}$ in the composite has been ensured by XRD (Bruker, D8 ADVANCE ECO) and pure barium ferrite by (Regaku, miniflex-II, XRD, CuKα radiation (λ= 1.54Å) in the scattering range (2θ) of 10°-80°. The magnetic characterization were carried out by using VSM, PAR 155, USA) with an applied field range of ±6000 Oe. at room temperature. Scanning electron microscopy (SEM, FEI Quanta –200) was employed to examine the surface morphology. The S parameters S11 (S22), S12 (S21) of the composite were studied by vector network analyzer (VNA E8263B Agilent Technologies) in X-band (frequency range of 8–12 GHz) using two port measurement techniques.

IV. RESULTS AND DISCUSSION

The XRD patterns of barium ferrite have been shown in Fig. 1(a). The diffraction peaks have been observed at 2θ value of 30.55(d=2.923), 32.37(d=2.763), 34.19(d=2.620), 37.30(d=2.407), 40.42(d=2.228), and 42.76(d=2.112), 55.49 (d=1.654), 57.05(d=1.612), 63.28(d=1.467) which corresponds hexagonal structured BaFe12O19 nanoparticles (JCPDS 12047-11-9). No diffraction peaks from other crystalline forms have been detected, which indicates a high purity and crystallinity of as-synthesized $BaFe_{12}O_{19}$ nanoparticles.

The crystallite size (D) of $BaFe_{12}O_{19}$ nanoparticles can be calculated by Scherrer's equation:

$$D = k\lambda/\beta\cos\theta$$

Where k is the shape factor, λ is the X-ray wavelength, θ is the Bragg angle (in degrees) and β is the full width at half maxima (in radians). The value of k is assigned as 0.89, which depends on various factors including the shape of the crystal and the Miller index of the reflecting plane. The crystallite size of $BaFe_{12}O_{19}$ particles has been calculated using above equation and evaluated to be50–70 nm, which is in pursuance of the HRTEM results
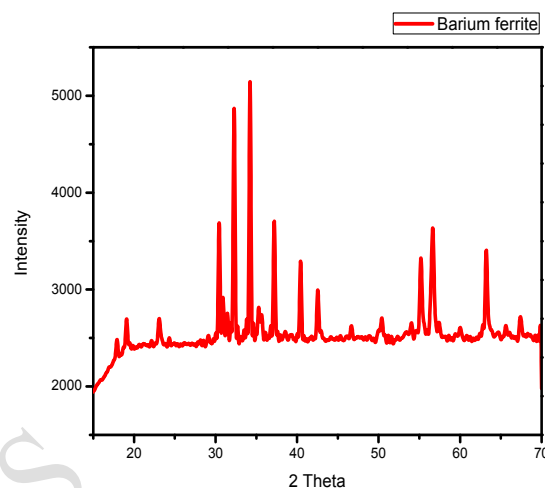

Figure 1: XRD patterns of $BaFe_{12}O_{19}$

The surface morphologies of $BaFe_{12}O_{19}$ nanoparticles were investigated using SEM. Fig. 2 (a) & (b) shows SEM images of $BaFe_{12}O_{19}$ nanoparticles.

It can be seen that $BaFe_{12}O_{19}$ nanoparticles are highly aggregated. The morphology and particle size distribution were determined by means of TEM. Fig. 2(c) & (d) shows the representative TEM image of the pure ferrite nanocrystals obtained from citrate precursor method. It can be seen in Fig.2(c) that $BaFe_{12}O_{19}$ nanoparticles are highly aggregated with an average particle size in the range of 50-70 nm. Fig. 2(d) shows the lattice plane spacing of barium ferrite particles, which is about 0.37 nm.
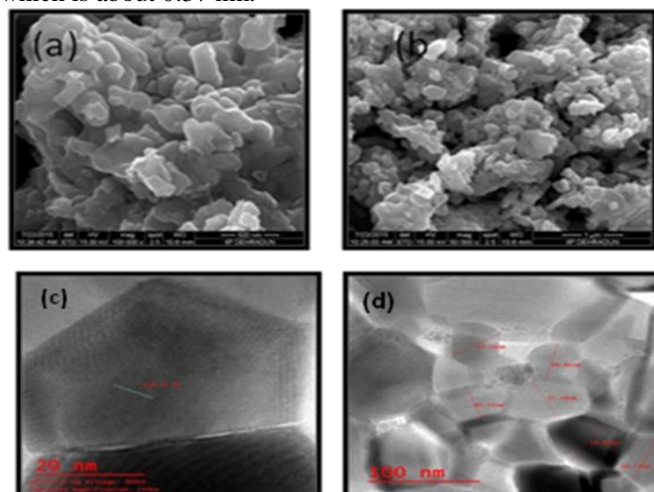

Figure 2: (a) & (b) SEM images (c) & (d) TEM images of $BaFe_{12}O_{19}$ nanoparticles

The magnetization curve of $BaFe_{12}O_{19}$ is measured at room temperature are exhibit in Fig.3. The magnetization (Ms) value of $BaFe_{12}O_{19}$ was found to be 52.084 emu/g at an external field of 9.5 kOe.
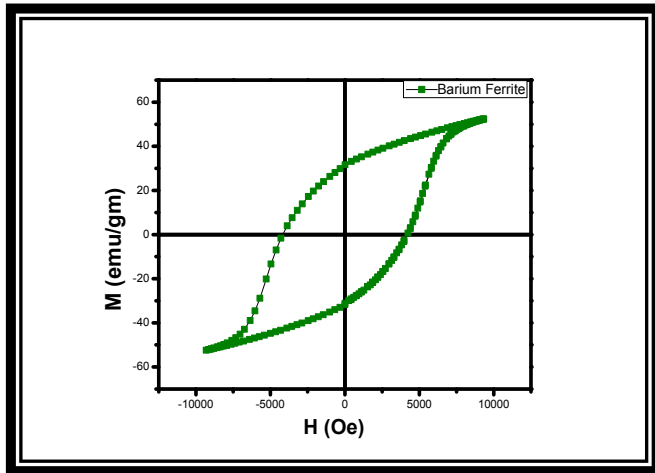

Figure 3: VSM of $BaFe_{12}O_{19}$ nanoparticles

V. EMI SHIELDING ANALYSIS

The EMI shielding effectiveness (SE) of a material is articulated in terms of ratio of incident and transmitted energy and can be mathematically expressed in logarithmic scale as:

$$SE (dB) = -10 \log (P_T/P_I) = SE_R + SE_A + SE_M$$

Where P_T and P_I are the transmitted power and incident EM waves respectively. There are three mechanisms contributing to the effectiveness of a shield. Part of the incident radiation is reflected from the front surface of the shield, part is absorbed within the shield material and part is reflected from the shield rear surface to the front. Therefore, the total shielding effectiveness of a shielding material (SE) equals the sum of the absorption factor (SE_A), the reflection factor (SE_R) and the correction factor to account for multiple reflections (SE_M) in thin shields given by

$$SE (dB) = SE_A + SE_R + SE_M$$

and can be expressed as

$$SE_R = -10 \log (1 - R)$$
$$SEA = -10 \log (1 - A_{eff}) = -10 \log (T/1 - R)$$
$$SEM = -20 \log (1 - e-2t/\delta) = -20 \log (1 - 10–SE_A /10)$$

Whereas SE_M is multiple reflection between both faces of shield and can be neglected when $SE_A > 10$ dB. Therefore, the effective absorbance (A_{eff}) can be manifested as $A_{eff} = (1 - R - T)/ (1-R)$ with respect to the power of the incident EM wave inside the shielding material.

Fig.4 exhibits the variation of (a) Shielding effectiveness (b) Real & imaginary part of permittivity (c) Real & imaginary part of permeability and (d) Tangent loss as a function of frequency.

Fig.4 (a) shows the dependence of the EMI SE within the 8.2–12.4 GHz frequency range. From the experimental measurement the shielding effectiveness due to reflection, absorption and total shielding effectiveness for barium ferrite is found to be, 5.7 dB, 0.25dB and 6.00 dB respectively. The complex parameters i.e. permittivity ($\varepsilon^* = \varepsilon'- i\varepsilon''$) and permeability ($\mu^* = \mu'- i\mu''$) of barium ferrite were investigated. The imaginary part (ε'') of dielectric constant is a measure of

dissipated energy and the real part (ε') is mainly associated with the amount of polarization occurring in the material. The dielectric performance of the material depends on orientational, electronic, ionic and space charge polarization [23]. Value of real part of permittivity is found to be vary from 5.5 to 6.9 and of imaginary part is 0.22 to 0.50 [Fig.4(b)].
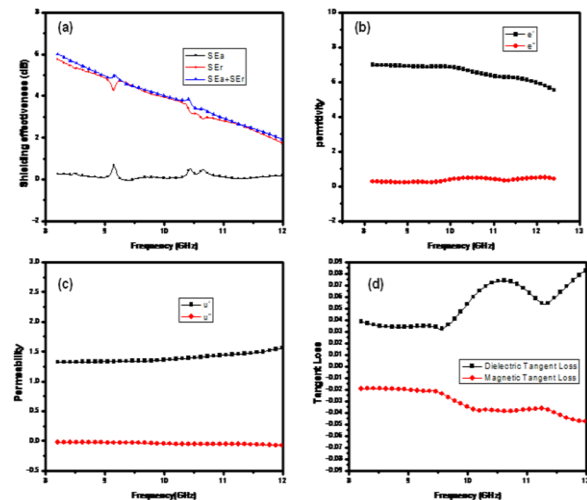

Figure 4: Variation of (a) Shielding effectiveness (b) Real & imaginary part of permittivity (c) Real & imaginary part of permeability and (d) Tangent loss as a function of frequency

The ratio of the imaginary to the real part ($\varepsilon''/\varepsilon'$) is the dielectric tangent loss which is represented by $\tan\delta E$ which denotes the angle between the voltage and the charging current. The observed $\tan\delta_E$ is always greater than 0.03 in the entire frequency range [Fig.4 (d)]. The values of μ' are in the range of 1.32 – 1.68, meanwhile, the values of μ'' are in the range of -0.06 to -0.02 [Fig 4(c)]. The magnetic tangent loss ($\tan \delta_M = \mu''/\mu'$) of barium ferrite also calculated using the permittivity and permeability parameters of the samples and presented in Fig. 4(d).

VI. CONCLUSIONS

Barium ferrite nanoparticles were successfully synthesized by citrate precursor method and its EMI shielding behavior was studied within the X-band (8.2–12.4 GHz) frequency range. The maximum shielding effectiveness observed was about 6 dB. The high values of saturation magnetization (52.084 emu/g) shows that it can used as a filler material in conducting polymer matrix for enhancement in its shielding effectiveness.

ACKNOWLEDGEMENTS

REFERENCES

[1] M. R. Meshram, N. K. Agrawal, B. Sinha, P. S. Misra, J. Magn. Magn. Mater. 271 (2004) 207.

[2] S. Sugimoto, S. Kondo, K. Okayama, D. Book, T. Kagotani, M. Homma, IEEE Trans. Magn. 35 (1999) 3154.

[3] Yuan CL, Hong YS, Lin CH (2011) Synthesis and characterization of Sr(ZnZr)xFe12-2xO19-PANI composites. J Magn Magn Mater 323:1851–4

[4] Cao MS, Song WL, Hou ZL, Wen B, Yuan J (2010) The effects of temperature and frequency on the dielectric properties, electromagnetic interference shielding and microwave-absorption of short carbon fiber/silica composites. Carbon 48:788–96

[5] Liu G, Zhang SJ, Jiang WH, Cao WW (2015) Losses in ferroelectric materials. Mat Sci Eng R 89:1–48

[6] Chang HY, Cheng SY, Sheu CI (2008) Microwave sintering of ferroelectric PZT thick films. Mater Lett 62:3620–2

[7] Gairola SP, Verma V, Kumar L, Dar MA, Annapoorni S, Kotnala RK (2010) Enhanced microwave absorption properties in polyaniline and nano-ferrite composites in X-band. Synth Met 160:2315–8

[8] Lakshmi K, John H, Mathew KT, Joseph R, George KE (2009) Microwave absorption, reaction and EMI shielding of PU-PANI composites. Acta Mater 57:371–5

[9] Tang JH, Ma L, Tian N, Gan MY, Xu FF, Zeng J et al (2014) Synthesis and electromagnetic properties of PANI/PVP/CIP core–shell composites. Mater Sci Eng B 186:26–32

[10] Yuan CL, Hong YS, Lin CH (2011) Synthesis and characterization of Sr(ZnZr)xFe12-2xO19-PANI composites. J Magn Magn Mater 323:1851–4

[11] Cao MS, Song WL, Hou ZL, Wen B, Yuan J (2010) The effects of temperature and frequency on the dielectric properties, electromagnetic interference shielding and microwave-absorption of short carbon fiber/silica composites. Carbon 48:788–96

[12] Fan M, He ZF, Pang H (2013) Microwave absorption enhancement of CIP/PANI composites. Synth Met 166:1–6

[13] K. Hatakeyama, T. Inui, IEEE Trans. Magn. 20 (5) (1984) 1261.

[14] Graeser M, Bognitzki M, Massa W, Pietzonka C, Greiner A and Wendorff J H 2007 Adv. Mater. 19 4244

[15] Yan L, Wang J B, Han X H, Ren Y, Liu Q F and Li F S 2010 Nanotechnology 21 095708

[16] Bobzin K, Schlaefer T, Begard M, Bruehl M, Bolelli G, Lusvarghi L, Lisjak D, Hujanen A, Lintunen P, Kanerva U, Varis T and Pasquale M 2010 Surf. Coat. Technol. 205 1015

[17] Li J, Zhang H W, Li Y X, Liu Y L and Ma Y B 2012 Chin. Phys. B 21 017501

[18] N. Shams, X. Liu, M. Matsumoto, A. Morisako, Manipulation of crystal orientation and microstructure of barium ferrite thin film, Journal of Magnetism and Magnetic Materials 290-291 (2005) 138-140.

[19] O. Carp, R. Barjega, E. Segal, M. Brezeanu, Nonconventional methods for obtaining hexaferrites, Thermochimica Acta 318 (1998) 57-62.

[20] J. Ding, W.F. Miao, P. G. McCormick, R. Street, Highcoercivity ferrite magnets prepared by mechanical alloying, Journal of Alloys and Compounds 281 (1998) 32-36.

[21] A. Mali, A. Ataie, Structural characterization of nanocrystalline BaFe12O19 powders synthesized by sol-gel combustion route, Scripta Materialia 53 (2005) 1065-1075.

[22] M. H. Makled, T. Matsui, H. Tsuda, H. Mabuchi, M. K. El- Mansy, Magnetic and dynamic mechanical properties of barium ferrite-natural rubber composites, Journal of Materials Processing Technology 160 (2005) 229-233.

[23] Expanded graphite–nanoferrite–fly ash composites for shielding of electromagnetic pollution. Monika Mishra, Avanish Pratap Singh, S.K. Dhawan, Journal of Alloys and Compounds 557 (2013) 244–251